

DEFORMATION MEASUREMENT OF A FLEXIBLE BIRDLIKE AIRFOIL WITH OPTICAL FLOW

Xiaoliang GONG¹, Stephan BANSMER²

¹*Northwestern Polytechnical University, Xi'an, China;* ²*Technische Universität
Braunschweig, Braunschweig, Germany*

Email: xianggong@gmail.com

Abstract

The application of the Lucas-Kanade (LK) optical flow technique has seen a huge success in a wide variety of fields. The goal of this paper is to apply the Lucas-Kanade technique in the measurement of the deformation of a flexible birdlike airfoil due to steady aerodynamic loads at transitional low Reynolds-numbers with single pixel resolution. To allow for large displacements, a pyramidal scheme is used to implement a coarse-to-fine warping strategy. To preserve discontinuities in the optical flow field, a nonlinear structure tensor is employed to diffuse local data anisotropically. To remove outliers, median filtering is introduced after each iteration. To create a pattern on the airfoil for the deformation measurement, the upper surface of the airfoil is stochastic sprayed with ink dot pattern for easy capture by two cameras observed from two different angles above the airfoil. At last, a general result of wind tunnel experiments is selected out, two optical flow fields are calculated respectively on two images generated from each camera, and optical flow results are compared with image correlation results.

Key words: optical flow, flexible airfoil deformation, pyramidal Lucas-Kanade, nonlinear structure tensor, image correlation

INTRODUCTION

1. Flapping Flight

Over a million different species of insects fly with flapping wings to produce lift and thrust, and more than 10,000 different kinds of birds and bats flap their wings for locomotion (Dial, 1994). Apparently, the insuperable maneuverability and agility of flapping flight contributes to their evolutionary success. Although flapping flight is much more complex than fixed or rotary winged flight, there has been continuous and substantial interest in it since the very beginning of humans' dream of flying like birds, which has flourished abundant theoretical, experimental and numerical results over the past a few decades.

2. Airfoil deformation

In some cases, the flexibility of flapping wings can increase both thrust coefficient and propulsive efficiency (Heathcote et al., 2007), which is a result of complex force interactions between aerodynamic forces, elastic forces and inertial forces. Indeed, the maximum camber during one flapping stroke was found to vary from 8 to 12% (Oehme, 1970). In order to reveal the hidden mechanism behind these aeroelastic interactions and verify the numerical simulation based upon different assumptions, the measurement of model deformation has thus been of interest for quite many years. These techniques include videogrammetry (Johnson et al., 2009), and projection moiré interferometry (PMI) (Burner, 2000). However,

videogrammetry is limited to measurement in sparse points no matter by retro-reflective targets (Barrows, 2007) or projected coded targets, and PMI require that the surface of interest be diffuse. In this paper, we attempt to take the advantage of optical flow to realize the deformation measurement of an airfoil.

3. Optical Flow

Optical flow determines the velocity field of two dimensional image intensity motions with single-pixel resolution. There are two main methods: global intensity smoothing methods based on Horn-Schunck scheme (Horn et al., 1981), and local methods based on Lucas-Kanade scheme (Lucas et al., 1981). Both methods based on the assumption that the intensity of moving pixels is constant over a short duration, which is known as brightness constancy assumption. This assumption gives out the famous optical flow constant equation. By this single equation, however, is insufficient to recover the velocity field, which is the well-known aperture problem. To solve this problem, Horn-Schunck scheme assumes that the optical flow is globally varying smoothly with neighboring pixels that have nearly identical velocity, while Lucas-Kanade scheme assumes that the optical flow is locally constant with neighboring pixels in the same window sharing the similar motion. Accordingly, Horn-Schunck calculates a 100% dense flow and it is sensitive to noise. Lucas-Kanade, on the other hand, does not give a dense flow but offers relatively high robustness under noise (Bruhn et al., 2005).

Since the Lucas-Kanade optical flow method was first proposed in 1981, it has been developed into numerous variants and the most widely used technique in computer vision (Baker et al., 2004). The application of such a method has seen a huge success in a wide variety of fields. This paper applies the pyramidal Lucas-Kanade (Bouguet, 2000) in the measurement of the deformation of a flexible birdlike airfoil due to steady aerodynamic loads at transitional low Reynolds-numbers.

4. Calibration

Combined with a calibration, it's possible to transform optical flow information to the three-dimensional deformation of the airfoil. Pinhole model and polynomial model (Soloff, 1997) are the two calibration models having been widely used, and the former has been used a lot in Computer Vision community while the latter has often been used in PIV community. Because the image correlation calculated by Davis Software of LaVision used a modified polynomial model, we used it also in optical flow calibration for consistency. Another reason using polynomial model is that solving parameters in the polynomial model by the least square equation is much easier than solving external parameters and internal parameters in pinhole model.

OPTICAL FLOW TECHNIQUE

Let $I_1(x, y, t)$ denote 2D image intensity, where x and y is the location of local intensity and t is the present time. Let $I_2(x + dx, y + dy, t + dt)$ denote local intensity after short time duration dt . dx, dy is the displacement of local intensity. The goal of Lucas-Kanade is to minimize the sum of squared error between $I_1(x, y, t)$ and $I_2(x + dx, y + dy, t + dt)$ in an integration window w :

$$E(dx, dy) = \min \sum_{x, y \in w} [I_1(x, y, t) - I_2(x + dx, y + dy, t + dt)]^2 \quad (1)$$

After performing first order Taylor expansion on $I_2(x + dx, y + dy, t + dt)$, Equation (1) is simplified to:

$$E(dx, dy) = \min \sum_{x, y \in w} (I_x dx + I_y dy + I_t dt)^2 \quad (2)$$

In our case, only two consequent images are considered, so we set dt equal 1. Then dx, dy can be replaced with u, v respectively. Equation (2) can be rewritten into:

$$E(u, v) = \min \sum_{x, y \in w} (I_x u + I_y v + I_t)^2 \quad (3)$$

A minimum of E with homogeneous Neumann (reflecting) boundary condition satisfies $\partial_u E = 0$ and $\partial_v E = 0$, leading to a linear system:

$$\begin{bmatrix} \sum_{x, y \in w} I_x^2 & \sum_{x, y \in w} I_x I_y \\ \sum_{x, y \in w} I_x I_y & \sum_{x, y \in w} I_y^2 \end{bmatrix} \begin{bmatrix} u \\ v \end{bmatrix} = \begin{bmatrix} - \sum_{x, y \in w} I_x I_t \\ - \sum_{x, y \in w} I_y I_t \end{bmatrix} \quad (4)$$

At first sight, solving this linear system is quite easy. However, in practice this task can be trapped in a dilemma. Three difficulties exist. First, the system matrix can be singular. Such singular matrices would appear in two regions, one is the homogeneous region where intensity derivatives are close to zero, leading to two near-zero eigenvalues; the other is around edges where one spatial derivative predominates, leading to the smaller eigenvalue being close to zero. Normally, we can threshold out these 'bad' regions by measuring the eigenvalues (Barron, 1994). In our code, a small positive constant is added to the diagonal of the matrix to suppress too small eigenvalues which can be considered as 'noise'. Secondly, because all pixels within local window share the same velocity, this tends to blur discontinuities in optical flow field. We draw ideas from (Brox, 2002) to utilize nonlinear structure tensor to preserve flow discontinuities. Thirdly, the linearization of an essentially nonlinear problem maintains proper accuracy only for quite small displacement, say less than one pixel. With larger displacements, the pyramidal Lucas-Kanade method gives out reasonable result. It downsamples the original image with the factor 0.5 on each level and starts the optical flow computation at the coarsest image. The coarse solution is used as initialization for solving a refined image until step by step the full resolution image is solved (Bouquet, 2000). At last, the median filter was introduced at the end of each iteration to discard outliers. It was originally proposed by (Westerweel, 1993) in particle image velocimetry (PIV) postprocessing to detect spurious vectors. It was also proved to significantly improve optical flow result (Wedel, 2008).

EXPERIMENTAL SETUP

1. Wind Tunnel

The experiments were carried out at the low-speed Low-Noise Wind Tunnel, see Fig. 1. The inlet of the Eiffel-type tunnel is covered by a fleece mat 30 mm in thickness. Afterward, the air passes a straightener made out of aluminum honeycombs, 14 mm in diameter and 200 mm in length and then finally through a fine-mesh woven screen. In the large settling chamber, small-scale turbulence is dissipated, and a Boerger-type nozzle contracts the air at a 16:1 ratio. Consequently, the air has a very low turbulence level in the 400×600 millimeter sized test section. The wind tunnel is driven by a 4 kW, acoustically encapsulated, speed controlled three-phase asynchronous motor, which produces stable wind-tunnel speeds from 2 up to 20 meters per second. The diffuser is mounted on a rail system, which allows one to interchange modular test sections. The laboratory is lined with open-celled acoustic foam.

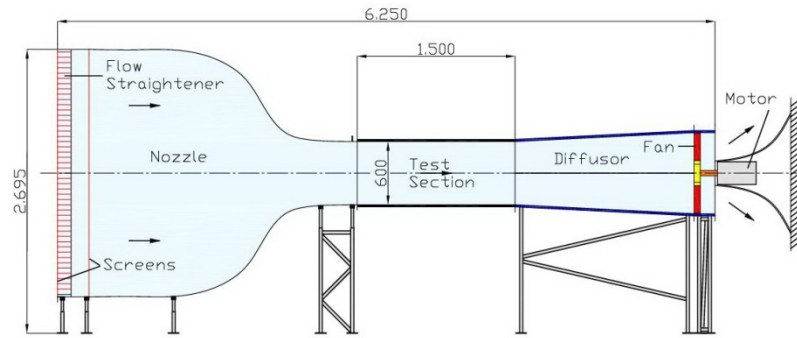


Fig. 1 Schematic of the low-speed Low-Noise Wind Tunnel.

2. Airfoil

The flexible airfoil used in this paper is the birdlike airfoil SG04 (Bansmer et al. 2010), see Fig. 2. It has been designed as a birdlike airfoil with two-dimensional behavior to study the coupled problem where the deformation of airfoil surface caused by aerodynamic and inertial loads. The dot pattern on the upper surface is stochastic ink spray for easy capture of airfoil motion by camera. The movement of this stochastic dot pattern and so the airfoil deformation is computed with optical flow.



Fig. 2 Flexible airfoil

3. Camera setup

The detailed camera setup is sketched in Fig. 3 as a side view of the wind-tunnel test section. The left oncoming air flows over the flexible airfoil with certain angle of attack. When the oncoming air flow is stable, the airfoil will be deformed. The Programmable Timing Unit (PTU9 by LaVision) is used to control a flash lamp to illuminate the airfoil, and two cameras in stereoscopic setup to photograph the ink pattern on the upper surface of the airfoil. This procedure is repeated with gradually increasing angle of attack, from 0 degree to 10 degree, and gradually increasing free stream velocity, from 0m/s to 8m/s. At last, we get two image series of the ink pattern for both cameras at different experimental status. After that we apply the pyramidal Lucas-Kanade optical flow algorithm to the two image series respectively to calculate two optical flow fields, i.e. the displacement of ink patterns.

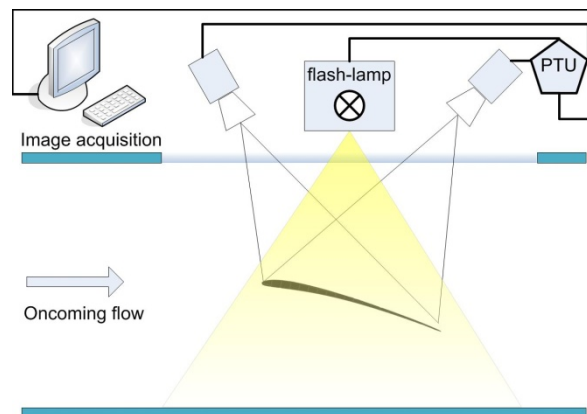


Fig. 3 Setup of the custom made deformation measurement system

DATA EVALUATION

1. Insight into optical flow result

In order to demonstrate the utility of our optical flow code, the synthetic sphere sequence¹ (Galvin et al., 1998) was selected. The sphere is rotating in the image sequence, while the background remains constant, see Fig. 4. The true flow field of this sequence is known, which makes the verification of optical flow much easier and more persuasive. Another more essential reason is that the spinning sphere consists of not only velocity regions having sharp discontinuities and continuous changes, but also image intensity having different discontinuous and continuous regions as velocity. This makes it possible for us to test the velocity discontinuity preserving property of the nonlinear structure tensor in intensity discontinuity regions, and to see what would happen when there is a velocity discontinuity in smooth intensity region or vice versa. An initial result is shown by color coded map in Fig. 4. The hue represents the orientation of the vector and brightness stands for its magnitude. The result is not identical to the true optical flow field, however, the preservation of discontinuity can be observed very well. But why there are several small slats cross the boundary in a periodical way? And why the worse situation happens at the up right corner?

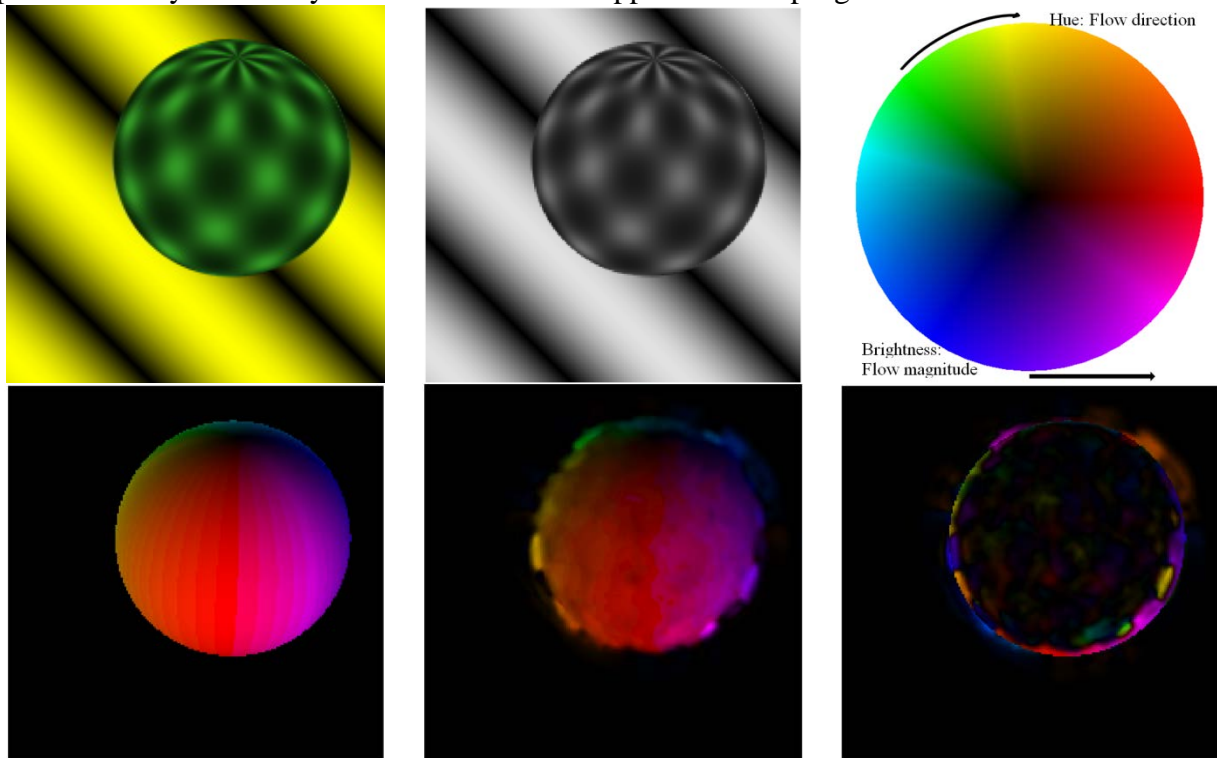


Fig. 4 Top LEFT: Original sphere sequence (Frame 1, 200×200 pixels). Top MIDDLE: Gray sphere sequence. Top RIGHT: The color code map. Bottom LEFT: Ground truth flow field. Bottom MIDDLE: Optical flow field. Bottom RIGHT: Error flow field.

The sphere sequence is a color image, however, since the camera used in the our experiments provides with only gray images, for consistency, the nonlinear structure tensor only takes the image gray difference into consideration. Thus, the above mentioned defect is predictable. Looking carefully at these places, we can find that the grayscale intensities within the ball are quite similar with their corresponding background neighbors. Inside the ball, the optical flow result is not smooth which can be explained by noticeable gray value discontinuities. However, if we set up the experiment carefully, problems discussed here can be avoidable, which can be demonstrated by the following comparison between image correlation and optical flow.

2. 2D flow field by optical flow and image correlation

To preliminarily verify optical flow, a small square region (200×200 pixels) was extracted from the original image (1024×1280 pixels) captured by camera one, see Fig. 5. On the left side, the trailing edge of the airfoil can be seen. The image correlation result is shown in Fig. 6. Again, the optical flow result is coded by color map, see Fig. 7.

The optical flow field captures left sharp discontinuity, benefiting from the fact that the image intensity and vector velocity share the same left boundary. The velocity within the extracted airfoil is smoother than that in sphere. This is because most of the discontinuous regions inside airfoil are in much smaller scale with respect of the scale of the airfoil. However, some discontinuous regions still affect the result.

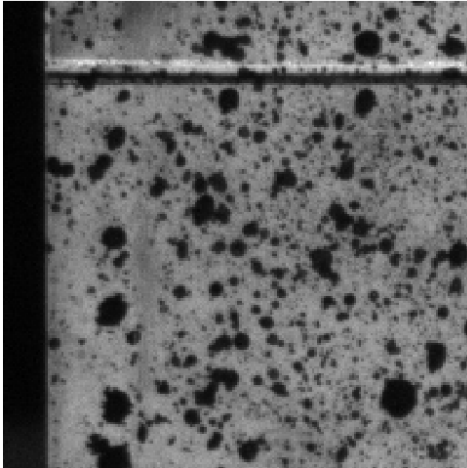


Fig. 5 Extracted airfoil

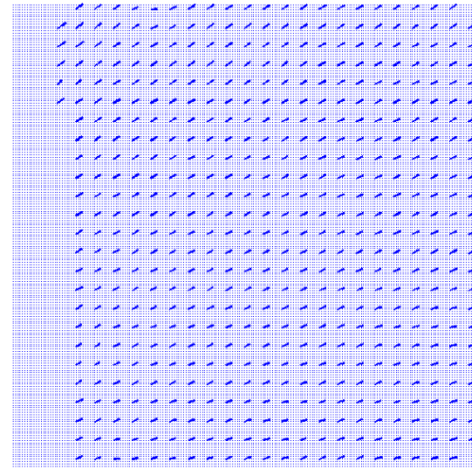


Fig. 6 Image correlation 2D flow field

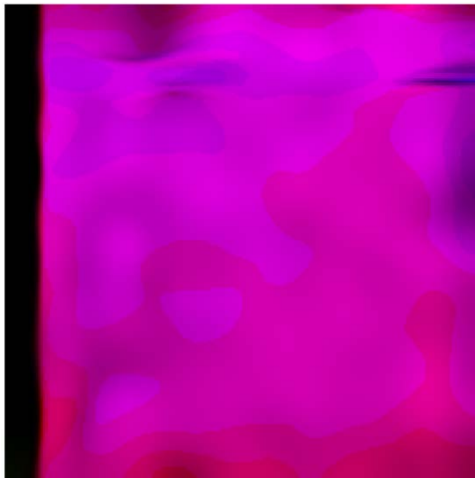


Fig. 7 Optical flow field

Table 1. Comparison between the PIV and optical flow

Measurement way	Error value
AE	4.3°
SD	2.87°
EE	0.10 pixel

Since the image correlation result gives an averaged flow vector over an area of 32×32 pixels, the correlation method is more insensitive to noise. Optical flow gives out a flow field with single pixel resolution.

The comparison is done in three ways: angular error (AE), standard deviation of angular error (SD) and endpoint error (EE).

AE was introduced by (Barron et al., 1994), and it is the most commonly used measure of performance for optical flow. The AE is calculated by measuring the angular difference between an estimated velocity $\mathbf{v}_e = (u_e, v_e, 1)$ and the correct velocity $\mathbf{v}_c = (u_c, v_c, 1)$:

$$AE = \arccos \left(\frac{u_c u_e + v_c v_e + 1}{\sqrt{u_c^2 + v_c^2 + 1} \sqrt{u_e^2 + v_e^2 + 1}} \right) \quad (5)$$

As an inherent property of the angular difference measurement, large and small speeds are treated without amplification. And AE can also handle “divide by zero” problem for zero flows. SD is the standard deviation of AE.

Sometimes it is desirable to compute EE used in Otte and Nagel (Otte et al., 1994), when we want errors in a region of large speeds are weighted more than errors in a region of small speeds. EE is defined as following:

$$EE = \sqrt{(u_c - u_e)^2 + (v_c - v_e)^2} \quad (6)$$

Results of the aforementioned three comparison methods can be seen in Table 1. All these results confirm the consistency between image correlation result and optical flow result.

3. Wing deformation by optical flow and image correlation

For present study, we selected the case at the angle of attack $\alpha=8^\circ$. Two images from two cameras are at 0m/s, and the other two are at 8m/s (which correspond to the investigated Reynolds number of 10000), see Fig. 8 top. Then the pyramidal Lucas-Kanade method was applied to the two images from each camera, after that, two optical flow fields were generated respectively, see Fig. 8 bottom. The velocity range (in pixel) for camera one is: $u_1 \in [-0.8, 3.5]$, $v_1 \in [-4.7, 1.9]$. The velocity range for camera two is: $u_2 \in [-21.0, 6.8]$, $v_2 \in [-5.3, 3.7]$. In this paper, except median filtering, no other postprocessing was used on optical flow result.

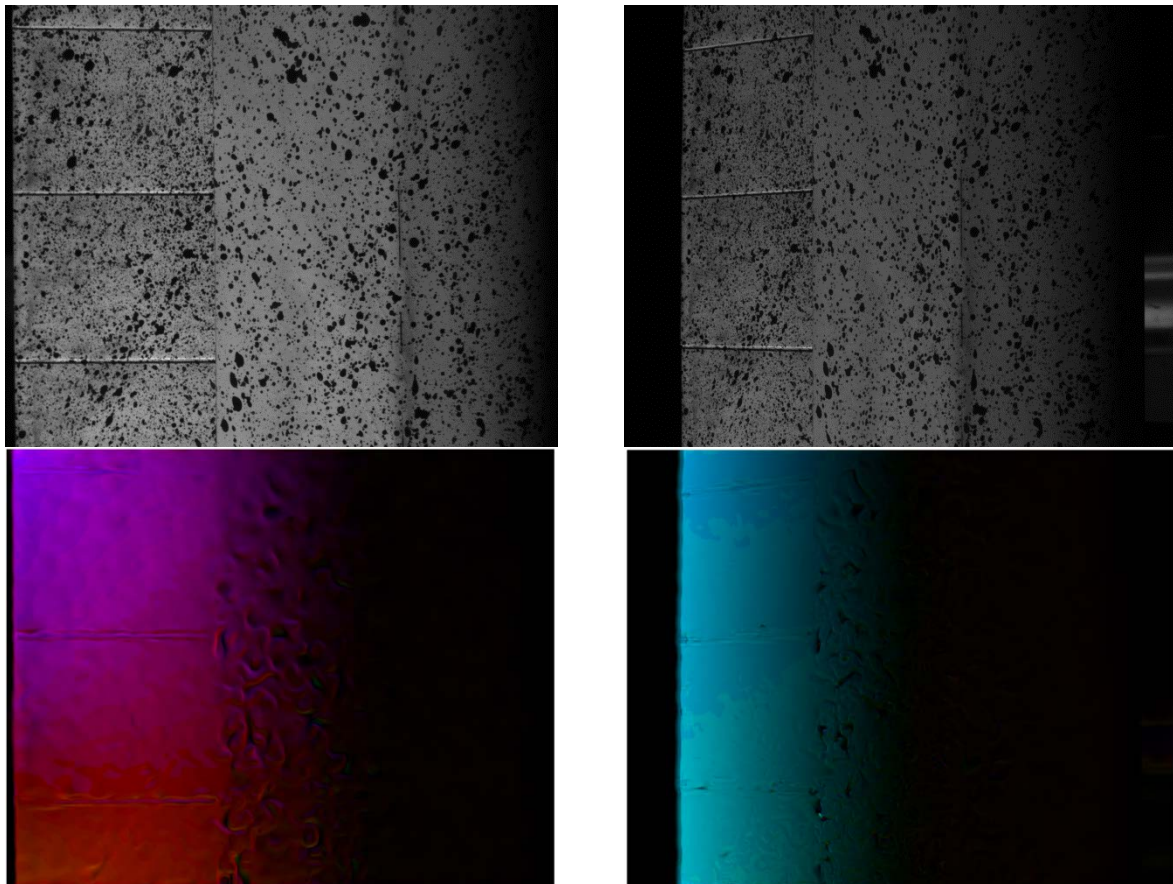


Fig. 8 Top LEFT: Image from camera one, 0m/s, $\alpha = 8^\circ$. Top RIGHT: Image from camera two, 0m/s, $\alpha = 8^\circ$. Bottom LEFT: 2D optical flow from camera one. Bottom RIGHT: 2D optical flow from camera two.

Sharp discontinuities were captured well, including the three straight lines representing the gaps between overlapping flexible shells. Since the ink spray in the middle part of the airfoil

is much sparser compared with the left flexible shells, apparent wrinkled patterns or black holes can be observed in the middle region while the left region is relatively smoother.

Then the calibration based on polynomial model was carried out. The polynomial has a cubic dependence in x and y , but a quadratic dependence in z . The calibration grid was inclined with the same angle of the chord line of the airfoil, and was translated to three z -positions with an interval of 10 mm, containing the whole range of airfoil deformation.

After calibration, we could reconstruct 3D velocity field from 2D optical flow filed. However, as the SG04 airfoil behaves in 2D way, the vertical deformation predominates in 3D displacements. This vertical deformation contour of the wing is shown in Fig. 9 top left. With a slice along the flow stream line, a curve displaying the vertical displacement of the airfoil can be plotted out, see Fig. 9 top right.

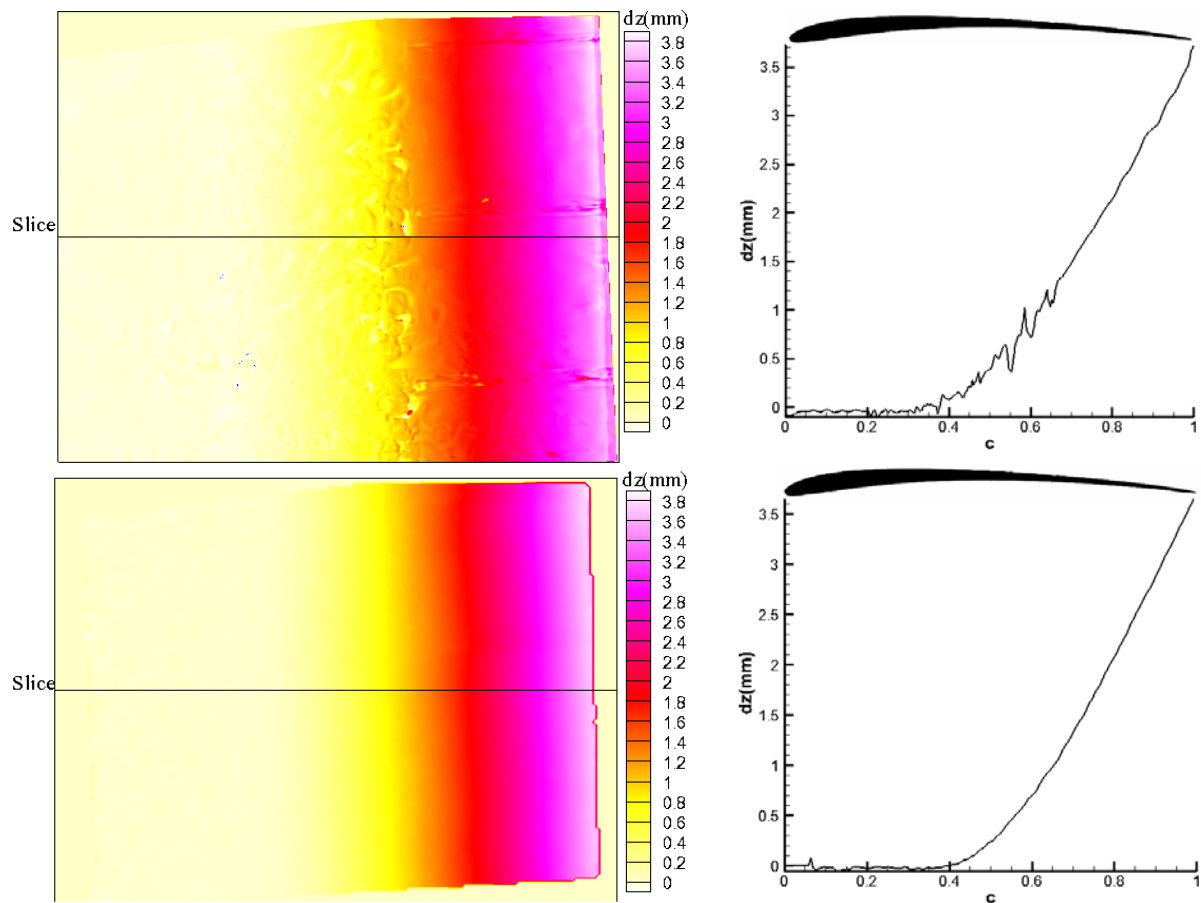


Fig. 9 LEFT: Vertical deformation contour of the 2D wing. RIGHT: Vertical deformation curve along the chord line. TOP: Optical flow result. BOTTOM: Image correlation result.

In order to verify optical flow result, stereoscopic cross-correlation was done using a multi-pass interrogation scheme with decreasing interrogation window size (from 128×128 pixels down to 32×32 pixels), 50% overlap and elliptical weighting function. The vertical deformation contour and vertical displacement along the chord line can be seen in Fig. 9 bottom.

On the one hand, the optical flow result and image correlation result share several common features. First of all, all figures show that near-zero deformation of the forebody is clear, which is in agreement with the airfoil design using carbon-reinforced plastic with a stiff forebody (Bansmer et al., 2010). Secondly, from deformation contours, it was shown that the wing deforms equally in spanwise direction. Thirdly, an exponential-like increment follows the undeformed region, reaching a highest value around 3.8 mm at the trailing edge. This deformation is considerable, regarding its scale and the low wind speed. So the flexibility of

wing should influence the aerodynamic properties a lot, which will be studied in future following research. Finally, look at two vertical deformation curves along the chord line carefully, Fig. 9 left, we can find that both curves experience oscillation to certain degree when the value is close to zero while both of them are smooth when the deformation is large, more precisely, above 1.2 mm. So both methods cannot compute too small deformation (around zero) accurately. For large deformation, both methods handle well.

On the other hand, the optical flow result and image correlation result have one obvious difference. Both of the deformation contour and curve manifests that optical flow fails to give satisfied smooth result in the middle part of the airfoil with the reason discussed above that the ink spray pattern in this part is too sparse. It should be no wonder that image correlation method could generate smooth result, because it used interrogation window size starting from 128×128 pixels which is, of course, big enough to ignore the defect of ink spray.

CONCLUSION

In this paper, the preliminary study on the deformation of a flexible birdlike wing by the pyramidal Lucas-Kanade optical flow method was done. The introduction of nonlinear structure tensor contributes to the preservation of velocity discontinuity regions where the image intensity is also discontinuous. The flexible airfoil was marked with a stochastic ink pattern. A stereoscopic camera setup was used to capture the motion of this pattern and thus the deformation of the airfoil. The pattern motion was well resolved with the present optical flow code. At last, the deformation of the birdlike wing was measured by stereoscopic image correlation and reconstructing the three-dimensional deformation from optical flow. It was shown that the wing deforms equally in spanwise direction. The deformation at the trailing edge at an angle of attack of 8 deg was determined to 3.8 mm. The image correlation gave smoother result than optical flow, this is because of the sparse ink spray and imperfect optical flow method. Nevertheless, the correlation scheme is limited in its spatial resolution by the size of the interrogation windows, 32×32 pixels in the present case. The optical flow code gives out single pixel resolution. Further research would be done in the future in order to improve the optical flow result in sparse pattern region. And more precise 3D reconstruction from 2D optical flow field would be studied as well.

Reference

- Dial, K.P. (1994): *An inside look at how birds fly: experimental studies of the internal and external processes controlling flight*, 1994 Report the Aerospace Profession, 38th Symposium Proceedings, The Beverly Hilton, Beverly Hills, CA.
- Heathcote, S., and Gursul, I. (2007): *Flexible Flapping Airfoil Propulsion at Low Reynolds Numbers*, AIAA Journal, Vol. 45, No. 5, pp. 1066–1079.
- Oehme, H., (1970): *Vergleichende Profiluntersuchungen an Vogel flügeln*, Beiträge zur Vogelkunde, Band 16, Heft 1/6.
- Johnson, J.T., Hughes, S., Dam, J.V. (2009): *A Stereo-Videogrammetry System for Monitoring Wind Turbine Blade Surfaces During Structural Testing*, Journal of ASME-Early Career Technical, Vol. 8, Num. 1, pp. 1.1-1.10.
- Burner, A. W., Fleming, G. A., and Hoppe, J. C. (2000): *Comparison of Three Optical Methods for Measuring Model Deformation*, 38th AIAA Aerospace Sciences Meeting and Exhibit, Reno, Nevada, AIAA 2000-0835, January 10-13.

- Barrows, D.A. (2007): *Videogrammetric Model Deformation Measurement Technique for Wind Tunnel Applications*, AIAA-2007-1163, 45th AIAA Aerospace Sciences Meeting and Exhibit, Reno, Nevada
- Westerweel, J. (1993): *Efficient detection of spurious vectors in particle image velocimetry data*. *Exp. Fluids*, Vol. 16, pp. 236 – 247.
- Wedel, A., Pock, T., Zach, C., Cremers, D., and H. Bischof. (2008): *An improved algorithm for TV-L1 optical flow*. In *Dagstuhl Motion Workshop*.
- Horn, B.K.P., Schunck, B.C. (1981): *Determining Optical Flow*, *Artificial Intelligence*, vol. 17, pp. 185-203
- Lucas, B., Kanade, T. (1981): *An iterative image registration technique with an application to stereo vision*, In *Proceedings of the International Joint Conference on Artificial Intelligence*, pp. 674–679
- Bruhn, A., Weickert, J., & Schnörr, C. (2005). *Lucas/Kanade meets Horn/Schunck: combining local and global optic flow methods*. *International Journal of Computer Vision*, 61(3), 211–231.
- Baker, S., Matthews, I. (2004): *Lucas-kanade 20 years on: A unifying framework: Part 1*. *International Journal of Computer Vision* 56(3), pp. 221–255.
- Bouguet, J. (2000): *Pyramidal Implementation of the Lucas Kanade Feature Tracker*, *OpenCV Documentation*, Intel Corporation, Microprocessor Research Labs
- Soloff, SM., Adrian, RJ., Liu, ZC. (1997): *Distortion compensation for generalized stereoscopic particle image velocimetry*. *Meas Sci Technol* 8:1441–1454
- Barron, J. L., Fleet, D. J., and Beauchemin, S. S. (1994): *Performance of optical flow techniques*. *International Journal of Computer Vision* , 12(1):43–77.
- Brox, T. and Weickert, J. (2002): *Nonlinear matrix diffusion for optic flow estimation*. In *Pattern Recognition*, L. Van Gool, (Ed.), vol. 2449 of *Lecture Notes in Computer Science* , Springer: Berlin, pp. 446–453.
- Bansmer, S., Radespiel, R., Unger, R., Haupt, M., Horst, P. (2010): *Experimental and Numerical Fluid-Structure Analysis of Rigid and Flexible Flapping Airfoils*, *AIAA Journal*, Vol. 48, No. 9, pp. 1959-1974.
- Galvin, B, McCane, B, Novins, K, Mason, D, and Mills, S. (1998): *Recovering motion fields: an analysis of eight optical flow algorithms*. In *Proc. 1998 British Machine Vision Conference*, Southampton, England.
- Otte, M., Nagel, H.-H. (1994): *Optical flow estimation: advances and comparisons*. In *Proceedings of the European conference on computer vision*, pp. 51–60.